Nanoscale Advances

PAPER

View Article Online
View Journal | View Issue

Cite this: *Nanoscale Adv.*, 2019, **1**, 4501

Observation of a novel double layer surface oxide phase on $Ni_3Al(111)$ at low temperature†

Xinzhou Ma,‡ Tim Kratky and Sebastian Günther *

The $Ni_3Al(111)$ surface was characterized during oxidation within the temperature range of 690–800 K by *in situ* scanning tunneling microscopy (STM), low energy electron diffraction (LEED) and auger electron spectroscopy (AES). Within this temperature range oxygen dosing always leads to the formation of a surface aluminum oxide layer while Ni atoms remain in their metallic state. The temperature however, affects the kinetics and the structure of the grown oxides. Above 790 K the known $(\sqrt{67} \times \sqrt{67})R12.2°$ double layer oxide grows, which consists of two Al–O layers. Oxygen dosing at the lower temperature of 740 ± 10 K leads to a single layer oxide with only one Al–O plane. The lattice mismatch of the aligned oxygen and substrate lattices induce a (7 × 7) moiré pattern of this surface phase. Surprisingly, when lowering the sample temperature below 720 K during oxygen exposure, again a bilayer oxide grows on the $Ni_3Al(111)$ surface. The formation of this bilayer oxide starts with the growth of the single layer oxide that is subsequently covered by a second Al–O layer. At temperatures close to 720 K, the 2nd layer is ordered and a diffraction pattern is observed indicating a $(4\sqrt{3} \times 4\sqrt{3})R30°$ unit cell with regard to the oxygen lattice of the surface oxide. A structure model is presented that relates this so far unknown double layer oxide to the building principle of α-Al_2O_3. The respective growth kinetics and the availability of Al atoms dictate whether the single or the low temperature double layer oxide is formed. The related mass transport on the surface can be observed using *in situ* STM which allows the qualitative discussion of the growth kinetics. When lowering the oxide growth temperature below 700 K, the 2nd oxide layer is still formed ontop of the single layer oxide but in a disordered state so that the LEED pattern of the single layer oxide with a (7 × 7) moiré unit cell is again observed. This accounts for the confusing fact that the (7 × 7) moiré LEED pattern may indicate either the formation of a single or a low temperature double layer oxide.

Received 30th August 2019
Accepted 12th October 2019

DOI: 10.1039/c9na00545e

rsc.li/nanoscale-advances

Introduction

Ni_xAl_y alloys are technically important because they are corrosive resistant metals with a particular high melting point and low specific weight.[1–3] The corrosive resistance originates from the formation of a protective oxide layer during oxidation as also found for other metal alloys. Especially, the mechanical stability of the protecting oxide layer is of great technological importance.[4,5] Due to this interest, the oxidation of Ni_xAl_y alloys has been thoroughly investigated since the late 80s, identifying the growth of a protective alumina film which accounts for the mechanical stability of the alloy under oxidative environment at high temperatures.[1,3,6–15] There exist five stable Ni_xAl_y alloys where the NiAl and Ni_3Al are the most studied and technically most relevant ones.[16] Especially NiAl is an exceptional material since it has a higher melting point (T_m = 1911 K) than Al (T_m = 933 K) and Ni (T_m = 1728 K).[17] The significantly larger heat of formation of Al_2O_3 (1675.7 kJ mol^{-1}) compared to the one of NiO (240.8 kJ mol^{-1})[6,17] indicates that the conversion of 1 mol O_2 towards Al_2O_3 is more than 2 times energetically more favorable than its conversion towards of NiO. Thus, from a thermodynamic point of view, it is expected that oxidation of NiAl alloys leads to the formation of alumina rather than nickel oxide. Indeed, on the low index planes of NiAl[9–13] and Ni_3Al[7,8,14,15] the formation of surface alumina films upon oxygen dosing at elevated temperature is reported.

Oxidation of Ni_xAl_y alloys provides a synthesis route towards the formation of well ordered ultrathin Al_2O_3 films. This preparation route cannot be performed on pure Al as only amorphous Al_2O_3 can be grown as thin layer, whereas the formation of crystalline Al_2O_3 on Al requires thicker layers or proceeds in island growth at high temperature.[18] The synthesis of well ordered oxide films on metallic substrates is used to produce model support surfaces for heterogeneous catalysts that may

Technische Universität München, Zentralinstitut für Katalyseforschung, Chemie Department, Physikalische Chemie mit Schwerpunkt Katalyse, Lichtenbergstr. 4, D-85748 Garching, Germany. E-mail: sebastian.guenther@tum.de

† Electronic supplementary information (ESI) available. See DOI: 10.1039/c9na00545e

‡ Current address: Foshan University, College of Materials Science and Energy Engineering, Foshan, 528000 Guangdong, P. R. China.

host metal clusters,[19,20] metal particles[21–27] and also metal oxide particles.[28–30]

The oxidation of $Ni_3Al(111)$[7,8,31–34] and especially the formation of the so called $(\sqrt{67} \times \sqrt{67})R12.2^\circ$ surface oxide is of great interest,[33,35] because it has nano-template properties that can be used to stabilize almost monodisperse distributions of metal particles on the thin alumina support.[34,36] While the evaporation of certain metals such as Pd and V was shown to lead directly to the formation of ordered arrays of mono disperse particles,[34,37] the synthesis of such arrays with other metals such as Fe and Au require a pre-evaporation step with a seeding metal.[34,38] The templating effect of the $(\sqrt{67} \times \sqrt{67})R12.2^\circ$ surface oxide was theoretically investigated in a systematic study with respect to the seeding of Fe, Co, Ni, Cu, Pd, Ag and Au[39,40] and this work was also recently reviewed.[41]

The $(\sqrt{67} \times \sqrt{67})R12.2^\circ$ surface phase was identified as a pure alumina layer on $Ni_3Al(111)$ consisting of two Al–O layers with a large and complicated unit cell.[31–33] Schmid *et al.* eventually derived a structure model for this surface oxide that mainly follows the building principles of α-alumina (corundum) being in agreement with a later photoelectron diffraction study.[34,42] The surface oxide consists of an Al_i–O_i interface layer that mainly follows the stoichiometry of corundum and which is rotated by about 23° with respect to the lattice of the metal support. The interface layer is covered by a second Al_{top}–O_{top} layer with the Al_{top} atoms situated above the O_i sites. The complicated unit cell of the surface oxide arises due to the presence of certain defects and lattice distortions in both Al–O layers that allow the surface atoms to relax and enlarge their lattice spacing. In the following, we will call the arrangement of the surface oxide consisting of two Al–O layers a bilayer or double layer oxide. The oxidation of the $Ni_3Al(111)$ was followed as a function of temperature within the temperature range of 600 K to 1050 K. In contrast to the formation of the $(\sqrt{67} \times \sqrt{67})R12.2^\circ$ surface phase upon oxygen exposure at about 1000 K which was attributed to a $(\sqrt{3} \times \sqrt{3})R30^\circ$ superstructure at that time,[8] it was found that the oxidation of $Ni_3Al(111)$ at about 800 K leads to an aluminum surface oxide with a (7×7) unit cell.[7,8,43] It was speculated that this surface oxide layer consists of a single Al–O layer only,[43] which could be confirmed recently.[44] In the latter study, the single layer oxide was shown to be formed as the main surface phase within the rather narrow temperature window of 740 K ± 10 K.

Although the oxidation of $Ni_3Al(111)$ has been investigated since more than 30 years, still no consistent picture exists on how the surface oxide formation actually takes place and which kinetic and thermodynamic restrictions favor the growth of the different surface oxide phases. Thus, we followed the formation of surface oxides on $Ni_3Al(111)$ upon the oxidation at temperatures between 690 K and 800 K by AES, LEED and *in situ* STM. We found that at temperatures above 750 K the well known $(\sqrt{67} \times \sqrt{67})R12.2^\circ$ bilayer oxide phase is formed in addition to the single layer oxide with the (7×7) moiré unit cell. At sufficiently high temperatures (above 790 K) the $(\sqrt{67} \times \sqrt{67})R12.2^\circ$ bilayer oxide phase appears as the only surface oxide on $Ni_3Al(111)$. Surprisingly, when lowering the temperature below 740 K during oxygen exposure, again another bilayer surface oxide grows ontop of the temporarily formed (7×7) single layer oxide. This novel bilayer oxide phase has not been reported so far in the literature. When dosing oxygen within a very narrow temperature window of 720 K ± 10 K, the low temperature double layer oxide grows as the major surface phase with a $(4\sqrt{3} \times 4\sqrt{3})R30^\circ$ unit cell when referring to the hexagonal oxygen lattice of the surface oxide phase. As will be shown in this study, we can relate the bilayer oxide phase to α-Al_2O_3 with the hexagonal oxygen lattice aligned with respect to the $Ni_3Al(111)$ lattice. The structural properties and the growth kinetics of the various surface phases will be discussed and related to the availability of surface Al atoms. It will be shown that the mass transport required for the buildup of the different surface oxides and the triggering nucleation events dictate which one of the various surface oxides grows on $Ni_3Al(111)$.

Experimental

The experiments were performed in a combined ultrahigh vacuum (UHV) system that consists of two vacuum chambers. One of the chambers hosts a high temperature scanning tunneling microscope (STM – SPECS Aarhus 150 HT-NAP), while the other offers surface preparation by ion etching and annealing together with Low Energy Electron Diffraction (LEED – Omicron Spectaleed) and Auger Electron Spectroscopy (AES – Staib DESA 100) as surface analysis techniques. Both chambers are connected and a transfer arm system can transport the sample from one chamber to the other. The sample temperature was measured in the STM- and the LEED/AES chamber by a Ni/NiCr thermocouple element which was connected to the side of the $Ni_3Al(111)$ single crystal. The thermocouple temperature reading was calibrated with the help of an IR-pyrometer (emissivity = 0.48). Oxygen exposure was performed either in the LEED/AES – or the STM chamber and both pressure gauges were calibrated with respect to each other.

All surface oxides reported in this publication and *in situ* STM oxygen dosing experiments were performed by adjusting an oxygen pressure of about 3×10^{-8} mbar and exposing the $Ni_3Al(111)$ surface up to the indicated dosage which never exceeded 200 L. However, oxygen dosing in the *in situ* STM experiments leads to an effective O_2 exposure about 6 times lower than expected from the indicated pressure reading. The lower O_2 impingement rate on the surface during *in situ* STM results from a thermo-shield that is positioned close to the hot sample in order to protect the STM scanner from radiative heating. Both, thermo shield and the STM tip reduce the impingement rate on the $Ni_3Al(111)$ surface by cutting a substantial part of the solid angle from which gas phase particles can reach the sample in a line of sight. In this study, we provide the oxygen dosage as read not trying to calibrate for the systematically larger reading of the *in situ* STM experiment because the effect of the thermo shield is not a geometric constant that can be accounted for but rather diminishes with time if the shield is saturated by adsorbed particles. As a result, during *in situ* dosing, very often an induction period is observed before the formation of a surface oxide phase appears.

Both UHV chambers have a background pressure in the low 10^{-10} mbar regime and during the *in situ* STM annealing experiments at $p(O_2) = 3 \times 10^{-8}$ mbar the background pressure remained below 10^{-9} mbar. Thus, the maximum possible H_2O pressure during oxygen exposure cannot exceed 10^{-9} mbar during all preparation steps and performed *in situ* experiments. All experiments were performed on clean $Ni_3Al(111)$ (sputter cleaned by several cycles of 10 min Ar^+ ion etching at 1.5 keV and a sample current of 3–4 μA) followed by annealing up to 1000 K. As a result, we can exclude potential slow accumulation of oxidic surface species and attribute all grown structures on the $Ni_3Al(111)$ surface to the applied oxygen exposure only. This is of importance, because Kelber *et al.* showed that water exposure at elevated pressure can lead to hydroxylated alumina species that are extremely temperature stable even under UHV conditions.[45] It was also shown that water exposure at 300 K to $Al_2O_3/Ni_3Al(111)$ within an intermediate pressure regime of 10^{-7} mbar < $p(H_2O)$ < 1 mbar induces substantial structural modifications of the thin oxide film when accumulating a water dosage of the order of 10^5 L.[45,46] However, it was shown that cooperative effects induced the reported surface modifications that were not seen at $p(H_2O)$ below 10^{-7} mbar at all. Taking into account that the potential water partial pressure during the performed experiments of this publication remained at least 2 orders of magnitude below the reported threshold value of 10^{-7} mbar and keeping in mind that the total oxygen exposure of the performed experiments never exceeded 200 L, we can safely rule out any water induced processes during the described oxidation of the $Ni_3Al(111)$ surface.

Results and discussion

As already noted in the Introduction, oxygen dosing at a narrow temperature window of 740 K ± 10 K leads to the growth of a single surface aluminum oxide layer on the Ni_3Al (111) surface as majority surface oxide phase. It is possible to cover the entire substrate surface with this phase. Fig. 1 displays the formation of this surface oxide on a terrace of the $Ni_3Al(111)$ surface which is surrounded by two adjacent monoatomic steps during oxygen dosing at 740 K. The image sequence (Movie in ESI-a†) shows the development of the surface layer proceeding towards the ascending and towards the descending step at the same time. It was shown that the single layer oxide layer consists of a hexagonally packed oxygen lattice aligned to the densely packed direction of the $Ni_3Al(111)$ substrate with a registry of 6 O-spacings of 2.94 Å on 7 next nearest-neighbor distances of the substrate (2.52 Å).[44] The resulting moiré of the surface oxide is imaged in STM with a characteristic vertical corrugation as a hexagonal pattern with a cell length of 17.6 Å (see contrast enhanced insets). When relating to the chemically ordered $Ni_3Al(111)$ surface the unit cell vectors have to be doubled in length so that the cell hosts 4 moiré waves. According to the Woods nomenclature the single layer surface oxide can then be considered as a (7×7) surface phase, although it was shown that the surface oxide may locally deviate from this structure.[44]

The hexagonally packed oxygen lattice of the (7×7) surface oxide was shown to host exclusively Al atoms that amount 0.5 ML when relating to the substrate packing density. This Al content of the single layer surface oxide agrees with occupation of 2/3 of the threefold oxygen coordinated sites by Al. The absence of additional symmetry within the (7×7) moiré cell led to the assumption that the Al atoms must be randomly distributed in the surface layer. The surface oxide phase was shown to grow within the metal terrace with the covering oxygen layer on top.[44] Thus, the contrast of the (7×7) surface oxide phase appearing slightly darker on the upper terrace must originate at least partly due to an electronic effect, indicating a reduced density of states (DOS) near the Fermi level compared to the metallic $Ni_3Al(111)$ surface. Note that the surface oxide growth imaged in Fig. 1 proceeds along straight growth fronts that are mainly aligned with the moiré pattern and thus support the building principle of the single oxide layer (also see movie and detailed description in ESI-a†).

Oxygen exposure on $Ni_3Al(111)$ at a slightly higher temperature leads to the formation of the well known $(\sqrt{67} \times \sqrt{67})$ R12.2° surface oxide layer. According to the structure model of Schmidt *et al.*, this surface phase is a double layer oxide consisting of a Al_{top}–O_{top} layer ontop of a so called interface Al_i–O_i

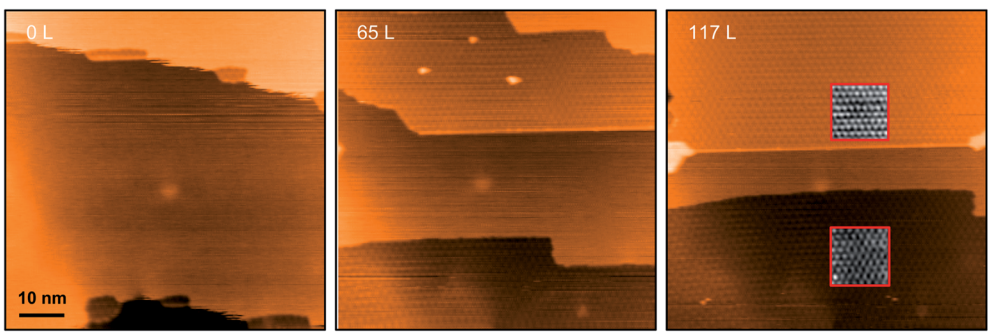

Fig. 1 $Ni_3Al(111)$ surface at $T = 740$ K after O_2 adsorption of 0 L (left), 65 L (middle) and 117 L (right) at $p(O_2) = 3.7 \times 10^{-8}$ mbar. The image sequence shows the almost entire coverage of the imaged area with the (7×7) single layer oxide phase. The moiré results from to the registry of 6 O–O distances on 7 next – nearest-neighbor substrate atom distances and appears in the STM image with a characteristic vertical corrugation (see contrast enhanced insets). Note that the growth front of the growing oxide phase proceeds along straight lines that are mainly aligned to the moiré. The movie (see ESI-a†) was acquired at $U = 0.85$ V and $I = 0.4$ nA.

layer.[34] The interface layer essentially consists of a hexagonally arranged O-layer with 2/3 of the threefold coordinated sites occupied by Al atoms. In contrast to the (7 × 7) single layer oxide the whole Al_i–O_i layer of the (√67 × √67)R12.2° surface phase is rotated by about 23° with respect to the underlying $Ni_3Al(111)$ lattice and the Al sites are well ordered forming a honeycomb lattice. The (√67 × √67)R12.2° surface oxide phase contains certain defects that lead to the complicated unit cell with a rotation angle of 12.2°. However, as has been argued by Schmidt *et al.* the double layer oxide very much relates to the building principle of α-Al_2O_3. Note that the O–O distance of 2.94 Å in the (7 × 7) single layer oxide[44] almost matches the one of 2.90 Å observed for chemisorbed oxygen on Al(111),[47] while the O–O spacing in the interface layer of the (√67 × √67)R12.2° double layer oxide is even expanded up to 3.02 Å.[34] Since the O–O distance in bulk corundum amounts 2.75 Å,[48] all surface oxide phases are strongly strained with a highly expanded lattice.

Fig. 2 shows an area of the crystal during *in situ* O_2 dosing at a temperature of 800 K, where exclusively the formation of the (√67 × √67)R12.2° oxide phase is observed. Although complete ordering is not achieved during *in situ* growth at this rather low temperature, the typical appearance of the (√67 × √67)R12.2° phase is observed when choosing a tunneling voltage below 1 V, where contrast is mainly affected by atoms of the interface layer. While STM imaging at U_t above 2 V provides the so called "network"- and the "dot"-contrast of the outermost oxide layer,[46] imaging at $U_t = 0.85$ V displays the (√67 × √67)R12.2° phase as dark features surrounded by white flowerlike protrusions (see inset of Fig. 2). Schmidt *et al.* noted that these flowerlike patterns occur if the oxygen atoms of the top layer are situated directly above the Al_i atoms of the underlying interface layer.[34]

The growth fronts of the (√67 × √67)R12.2° double layer oxide phase shown in Fig. 2 do not proceed along straight but rather kinked edges indicating the rotational misalignment of the surface oxide and the underlying substrate. The image sequence of Fig. 2 (movie in ESI-b†) proves that this growth mode along kinked edges results in a seemingly random outward growth of the double layer oxide from the former step edges together with an inward growth on the terrace until finally the whole terrace is covered by the oxide phase. Thus, dosing O_2 to the $Ni_3Al(111)$ surface at temperatures more than 60 K above the formation temperature of the (7 × 7) single layer oxide (740 K) leads to the growth of the (√67 × √67)R12.2° double layer oxide.

Surprisingly, a new double layer oxide phase is formed during *in situ* O_2 dosing also when lowering the temperature slightly below the single layer oxide growth temperature of 740 K. Fig. 3 displays an image sequence during oxygen exposure up to 100 L at 720 K (movie in ESI-c†).

The data set shows that oxygen dosing leads to the nucleation and growth of dark, triangular islands with the typical moiré of the (7 × 7) single layer oxide. The dark appearance of the (7 × 7) surface oxide islands on the metallic terrace results from spectroscopic contrast due to a reduced DOS when compared to the surrounding metallic terrace. In few cases, white islands are nucleated on top of the (7 × 7) single layer oxide patches. Within an intermediate dosing time (between 46 L and 66 L) a large amount of bright dots appears on top of the single layer oxide patches. The bright dots occupy sites in registry with the moiré corrugation. The amount of bright dots decreases after the 2nd layer area ontop of the (7 × 7) single layer oxide starts to grow in size (after the dosage of 67 L). Contrast enhanced gray scale insets in Fig. 3 (at 55 L and 67 L) point out the appearance and disappearance of the bright spots. While continuing the oxygen exposure, finally, almost all single layer oxide islands are covered with 2nd layer material and appear as bright islands on top of the dark triangles.

White arrows displayed in the STM images of Fig. 3 indicate the densely packed directions of the $Ni_3Al(111)$ crystal to which all triangular single layer oxide islands are aligned and to which also the covering 2nd layer aligns. It is tempting to relate the white dots and the covering 2nd layer to the material required for the formation of a double layer surface oxide. It has been shown that the formation of the (7 × 7) single layer oxide phase releases metal atoms from the substrate that have to be laterally displaced on the $Ni_3Al(111)$ surface.[44] However, the formation of a 2nd layer on top of the single layer oxide requires metal atoms that have to be taken from somewhere. In the following we will

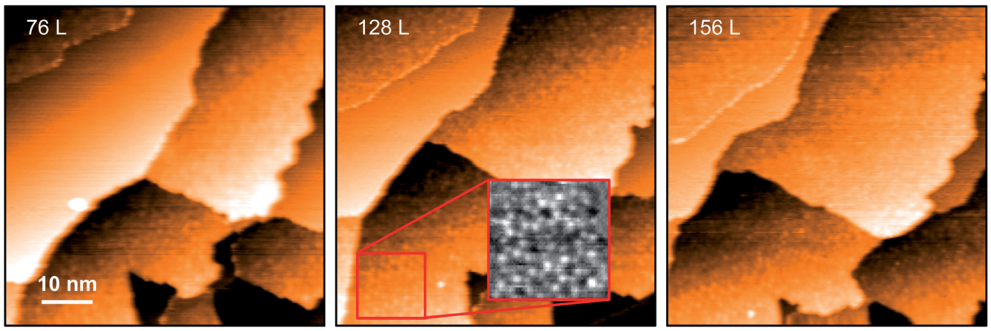

Fig. 2 Double layer oxide growth at 800 K with a defective (√67 × √67)R12.2° structure after O_2 adsorption of 76 L (left), 128 L (middle) and 156 L (right) at $p(O_2) = 3.5 \times 10^{-8}$ mbar. Although highly defective, the typical appearance of the (√67 × √67)R12.2° unit cell with dark protrusions surrounded by bright flower like features is observed (see contrast enhanced inset). Note that the surface oxide grows in islands with kinked edges. The movie (see ESI-b†) was acquired at $U = 0.85$ V and $I = 0.4$ nA.

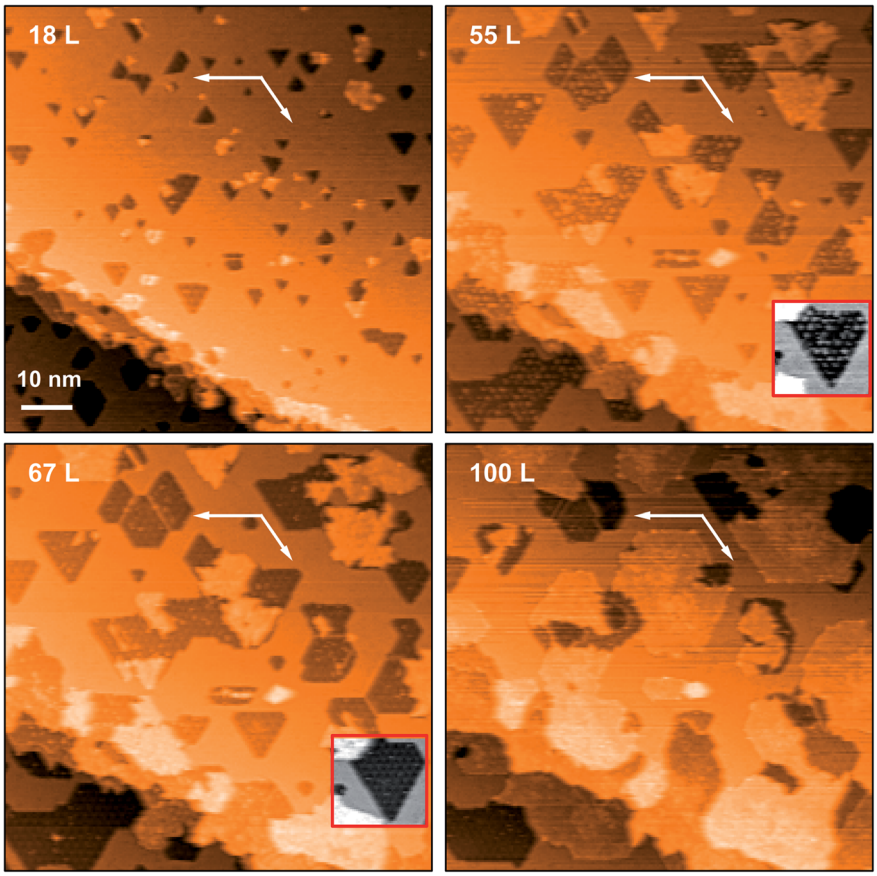

Fig. 3 Double layer oxide growth at 720 K after O_2 dosing of 18 L, 55 L, 67 L and 100 L at $p(O_2) = 3.0 \times 10^{-8}$ mbar. At first, the (7 × 7) single layer oxide phase is formed which appears as dark, triangular islands with the characteristic corrugation of the moiré. Temporarily, after having dosed 46–66 L bright dots appear ontop of the (7 × 7) single layer oxide patches. The bright dots disappear after the 2nd layer oxide growth ontop of the single layer oxide proceeds at higher speed. Gray scale insets show contrast enhanced parts of the images at 55 L and 67 L and indicate the dynamics of the bright spots. Finally, all (7 × 7) single layer oxide patches are covered with a 2nd layer and are imaged as bright islands in STM (see 100 L image). White arrows indicate the crystallographic directions of the substrate to which both, the single and the double layer islands align. The movie (see ESI-c†) was acquired at $U = 0.85$ V and $I = 0.5$ nA.

show that the 2nd layer of the low temperature surface oxide consists of alumina and we will address the issue of material transport again further below.

Auger spectra acquired from the $Ni_3Al(111)$ surface after dosing 170 L oxygen at 720 K can be used to identify the chemical nature of the low temperature double layer surface phase. Fig. 4 displays the corresponding spectra at low (40–75 eV) and high kinetic energy (450–900 eV) in comparison to the ones obtained from the clean $Ni_3Al(111)$ surface and the one covered by the (7 × 7) single layer oxide phase. In the low electron energy regime the Al peak at 68 eV relating to metallic Al is observed only in the dN/dE curves obtained from the clean $Ni_3Al(111)$ surface while it is absent after oxidation at 720 K and 740 K. Instead, the Al peak at 51 eV appears after oxygen dosing indicating the formation of aluminum oxide. Note the more pronounced Al-oxide peak after oxidation at the lower temperature. Also note that the Ni peak at 61 eV remains almost unchanged in the spectra acquired from all three samples (the slight peak shape change results from the overlap with the Al related peaks). The fact that Ni is not affected by oxygen dosing is evidenced by the peaks of the Ni(LMM) transitions shown in the right panel of Fig. 4 which do not show any change of their peak position or shape. Note that the formation of NiO is readily identified by a significant peak shift of >2 eV accompanied by a pronounced peak shape change,[49] which is explicitly shown by the data sets compiled in the ESI (see ESI-d†). Here, also the formation of a potential spinel phase with a $NiAl_2O_4$ stoichiometry upon oxygen exposure of the $Ni_3Al(111)$ surface at 740 K and at 720 K can be excluded. Thus, both surface oxide phases formed at 740 K and at 720 K leave the Ni atoms unaffected in their metallic state in accordance with the findings of Venezia and Loxton.[1]

Becker *et al.* suggested that the (7 × 7) moiré oxide phase consists of a single Al/O layer[43] which could be substantiated in our recent study where we determined the oxygen content of the (7 × 7) moiré surface oxide phase as 0.73 ML and the Al content as 0.5 ML.[44] We can now use this information to quantify the coverage of the low temperature surface oxide phase by comparing the respective auger electron peak intensities.

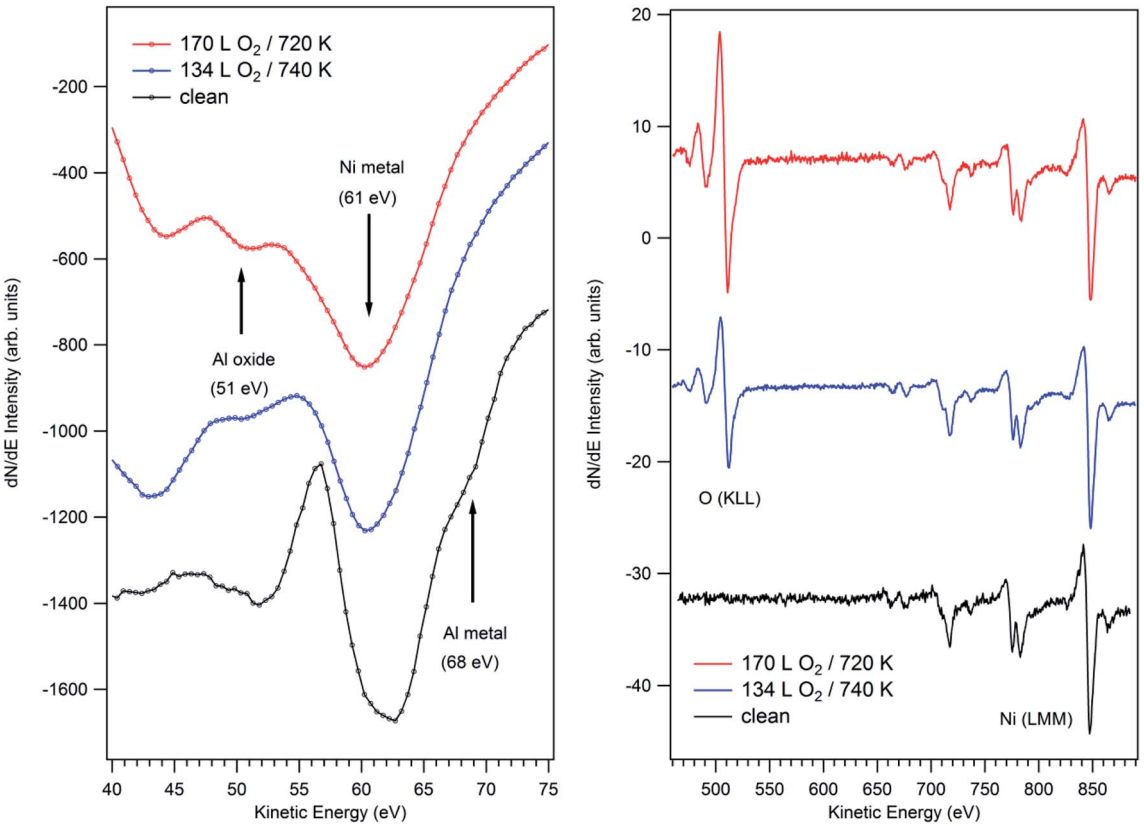

Fig. 4 AES spectra from the clean and oxidized $Ni_3Al(111)$ surface at 740 K (single layer oxide after the dosage of 134 L) and at 720 K (low temperature double layer oxide after the dosage of 170 L). Left panel: low energy AES peaks. The peak positions of the characteristic Al transitions indicative for metallic (68 eV) and oxidic Al (51 eV) and the peak position of the metallic Ni transition (61 eV) are indicated by arrows. Right panel: O(KLL) and Ni(LMM) Auger peaks. All spectra are scaled to the same Ni(LMM) intensity so that each O(KLL) peak size reflects the amount of oxygen in the structure. No change of the Ni(LMM) transitions regarding peak shape of peak position is observed. This finding proves that Ni is still present in the metallic state and thus, does not contribute to the formation of the surface oxide layer. The auger spectra were recorded with a primary electron energy of 3 keV.

In the right panel of Fig. 4 all displayed spectra are scaled to the same intensity of the Ni(LMM) transition and it is clearly visible that the O(KLL) peak of the low temperature oxide surface phase is significantly larger than the one obtained from the single layer surface oxide phase formed at 740 K. In fact, the scaled O(KLL)/Ni(LMM) intensity ratio exceeds the one of the (7 × 7) single layer oxide phase by a factor of 1.89. *I.e.* the oxide phase formed at 720 K contains about twice as much oxygen atoms than the single layer oxide.

In a recent publication, we could show that the damping of the Ni(LMM) signal during the formation of the (7 × 7) oxide phase is compatible with the formation of a single oxide layer.[44] Assuming that the second layer of the low temperature bilayer oxide contains the same amount of Al and O atoms as the first layer, we can compute the expected increase of the O(KLL)/Ni(LMM) intensity ratio obtained from the bilayer surface oxide and compare it to the respective value obtained from the (7 × 7) single layer oxide phase. Within the error bars of this calculation (see ESI-e†), the expected increase agrees well with the experimentally observed increase of 1.89.

The $Ni_3Al(111)$ surface develops three different low energy electron diffraction (LEED) patterns after oxygen dosing at low (720 K), medium (740 K) and high (800 K) temperature. The respective LEED patterns acquired at an electron energy of 60 eV are displayed in Fig. 5.

The LEED pattern of the high temperature ($T = 800$ K) oxide resembles the one of the well known $(\sqrt{67} \times \sqrt{67})R12.2°$ double layer oxide and the pattern displayed in the center panel of Fig. 5 ($T = 740$ K) is the one of the (7 × 7) single layer oxide phase. However, the LEED pattern of the surface oxide formed at lowest temperature ($T = 720$ K) is so far unknown. In addition to the pronounced (1,0) diffraction spots at the position of the oxygen lattice already observed in the LEED pattern of the (7 × 7) single layer oxide (see white arrow in the center and left panel of Fig. 5), diffraction spots appear at the positions that indicate a $(4\sqrt{3} \times 4\sqrt{3})R30°$ unit cell with respect to the (1,0) oxide spots. Also note that no substrate related diffraction spots appear in the pattern of the low temperature double layer oxide (as evidenced by comparison with the red arrows in the center panel of Fig. 5).

The (7 × 7) single layer oxide phase very much relates to the Al_i–O_i interface layer of the $(\sqrt{67} \times \sqrt{67})R12.2°$ double layer oxide except for the rotational alignment with respect to the substrate lattice. Schmidt *et al.* pointed out that the high

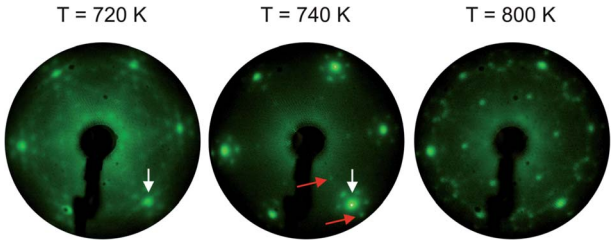

Fig. 5 LEED patterns acquired from the $Ni_3Al(111)$ surface after O_2 dosage of 162 L at $T = 720$ K (left), 134 L at $T = 740$ K (middle) and 166 L at $T = 800$ K (right). While the LEED pattern of the oxide formed at 740 K corresponds to the reported (7×7) single layer oxide and the one of the surface oxide grown at 800 K refers to the well known $(\sqrt{67} \times \sqrt{67})R12.2°$ double layer oxide, the LEED pattern of the low temperature double layer oxide shown in the left panel is so far unknown in the literature. Red arrows in the center panel indicate the position of the substrate diffraction spots relating to the next neighbor distance of 2.52 Å and the unit cell length of the $Ni_3Al(111)$ substrate which is twice as long. The white arrow indicates the (1,0) spot position of the hexagonal oxygen lattice of the single oxide layer moiré phase with a O–O distance of 2.94 Å. Comparison with the LEED pattern of the low temperature double layer oxide in the left panel evidences the absence of substrate related diffraction spots while the pronounced (1,0) oxide spots still appear (see white arrow). The additional spots indicate a $(4\sqrt{3} \times 4\sqrt{3})R30°$ unit cell when relating to the (1,0) oxide spots. All LEED patterns were acquired at an electron beam energy of 60 eV.

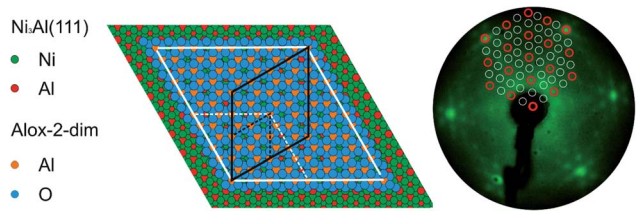

Fig. 6 Left: structure model of a double layer oxide with a hexagonally arranged oxygen lattice (blue spheres) aligned to the lattice of the Ni_3Al surface (green and red spheres) at a registry of 6 oxide units on 7 next neighbor distances of the $Ni_3Al(111)$ surface. If we apply the building principle of α-Al_2O_3 (corundum) with an ordered Al occupation of 2/3 of the octahedrally coordinated sites to the 2nd oxide layer the sketched Al honeycomb lattice (orange spheres) appears at the surface. The black unit cell of this structure indicates the $(2\sqrt{3} \times 2\sqrt{3})R30°$ unit (dashed black lines) or the $(4\sqrt{3} \times 4\sqrt{3})R30°$ unit (solid black lines) which is in accordance with the observed pronounced $(2\sqrt{3} \times 2\sqrt{3})R30°$ – (red circles) and the additional $(4\sqrt{3} \times 4\sqrt{3})R30°$ diffraction spots (white circles) of the LEED pattern. Note that the registry with the chemically ordered $Ni_3Al(111)$ surface is reached for the respective larger unit cell (for sake of better visibility the Al atoms of the interface layer are not sketched).

temperature $(\sqrt{67} \times \sqrt{67})R12.2°$ double layer oxide obeys the building principle of α-Al_2O_3.[34] Thus, it seems likely to assume that also the low temperature $(4\sqrt{3} \times 4\sqrt{3})R30°$ bilayer oxide phase relates to a sort of double layer α-Al_2O_3, but now with an oxygen lattice aligned to the $Ni_3Al(111)$ substrate lattice. The ordered occupation of 2/3 of the octahedrally O-coordinated sites in corundum by Al atoms naturally results in the formation of a Al honeycomb lattice which is 30° rotated with respect to the hexagonal oxygen lattice.[48] With the bilayer structure of the low temperature surface oxide supported by STM and AES data and the rotational alignment observed by STM and LEED, we can apply this building principle to the second layer of the low temperature surface oxide phase and derive the hard sphere model shown in Fig. 6.

In this model, we assume that the Al_i–O_i interface layer follows the building principle of the (7×7) single layer oxide with the Al atoms randomly distributed so that the interface layer follows the symmetry of the moiré due to the lattice mismatch of the O–O and the $Ni_3Al(111)$ substrate lattice. When assuming an ordered arrangement in the outermost Al_{top}–O_{top} layer of the bilayer oxide structure with 2/3 of the octahedrally O-coordinated positions occupied by Al, the Al honeycomb lattice in the second layer (orange spheres) naturally leads to the $(2\sqrt{3} \times 2\sqrt{3})R30°$ unit cell within the (6×6)-O-lattice cell (see the dashed black and white cell). When relating to a chemically ordered $Ni_3Al(111)$ support, the unit cell has to be four times enlarged revealing the $(4\sqrt{3} \times 4\sqrt{3})R30°$ unit cell with respect to the hexagonal oxygen lattice with a lattice constant of 2.94 Å (the respective cells are indicated by black and white solid lines). Note that for sake of better visibility the Al atoms of the interface layer are not sketched in Fig. 6 since we claim that they are distributed randomly.

The respective diffraction spots of a $(2\sqrt{3} \times 2\sqrt{3})R30°$ and a $(4\sqrt{3} \times 4\sqrt{3})R30°$ unit cell are indicated by red and white circles in the LEED pattern shown beside the hard sphere model of Fig. 6. They match very well the observed diffraction spots of the low temperature bilayer oxide which supports the suggested structure model. The hard sphere model of Fig. 6 is also supported by the fact that both, the low temperature bilayer and the single layer oxide form along straight aligned growth fronts while the high temperature $(\sqrt{67} \times \sqrt{67})R12.2°$ double layer oxide phase grows along kinked edges as expected for a rotated oxide layer.

Rarely, the low temperature double layer oxide can be found as a minority surface phase in coexistence with the (7×7) single layer oxide after having oxidized the $Ni_3Al(111)$ surface at elevated temperature. The coexistence of both oxides enables us to compare their structural appearance in STM images as shown in Fig. 7.

The STM image in the left panel of Fig. 7 displays the typical contrast of the moiré of the (7×7) single layer oxide phase as a hexagonal pattern with a periodicity of 17.6 Å, whereas the double layer oxide phase is imaged as a hexagonally array of protrusions with a lattice distance of about 10.2 Å and a lattice orientation rotated by 30° with respect to the moiré of the (7×7) single layer oxide. Indicating the protrusions of the double layer oxide by white circles and overlaying them on the (7×7) single layer oxide in the STM image proves an exact registry of 3 white circles along the $\sqrt{3}$-direction of the moiré beating frequency of the single layer oxide. Comparison with the hard sphere model displayed in the right panel of Fig. 7 indicates that one moiré cell hosts 6 Al honeycomb units along its $\sqrt{3}$-direction as highlighted by black hexagons. Why only 3 out of 6 honeycombs are imaged as protrusions cannot be resolved because it was not possible to record STM data at even elevated

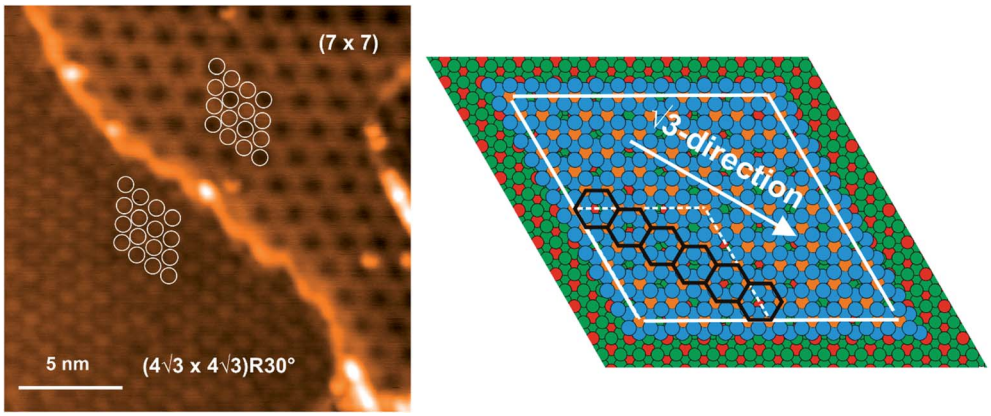

Fig. 7 Coexisting patches of the low temperature double layer oxide and the (7 × 7) single layer oxide locally formed on the $Ni_3Al(111)$ surface after dosage of 61 L O_2 at 750 K allow to compare the structural appearance of both phases in STM. Left: STM image of an area covered by the low temperature double layer oxide (lower left part) and the (7 × 7) single layer oxide (upper right part). White circles indicate the resolved corrugation of the double layer oxide. Overlay ontop of the imaged moiré of the (7 × 7) single layer oxide phase indicates that 3 units appear along the √3-direction of the moiré cell. Right: comparison with the structural model of Fig. 6 reveals that one would expect 6 honeycomb units (black hexagons) along the √3-direction of the moiré beating frequency. The STM image was acquired at $U = 0.72$ V and $I = 0.2$ nA.

lateral resolution. One possibility might be that the surface oxide is in registry with the substrate only at the corners of the moiré cell while along the √3-direction of the cell gradually ontop and bridge sites are populated and, as a result, not all honeycombs will be imaged equally. Of course, the observed contrast in the STM image might also result from a slight deviation from the building principle of α-Al_2O_3 such as the reconstruction of the outermost layer of the high temperature (√67 × √67)R12.2° double layer oxide phase.

Finally, we can discuss the driving forces that lead to the formation of the surface oxide phases. Fig. 8 displays the qualitative potential energy diagram for the formation of the three surface oxide phases. The panel above the diagram sketches the mechanisms required for the buildup of the respective phase. As a first process, the O_2 adsorption leads to the formation of mobile O_{ad} or $Al_xO_{y\text{-ad}}$ entities that induce the formation of the (7 × 7) single layer oxide phase in the surface of the $Ni_3Al(111)$ crystal. Within the temperature range of 740 K ± 10 K, this single layer oxide phase can be grown until it covers the entire surface of the crystal (see Fig. 1 and ref. 44). Thus, there must exist an energy barrier E_{B3} which prevents the growth of the (√67 × √67)R12.2° bilayer surface oxide which is the energetically more favorable oxide phase. Note that the (√67 × √67)R12.2° double layer oxide can be grown at higher temperatures directly on the metallic $Ni_3Al(111)$ surface and does not require the formation of the (7 × 7) single layer oxide (see Fig. 2). Thus, we conclude that the (√67 × √67)R12.2° bilayer oxide is thermodynamically more stable than the single layer surface oxide phase and that the (7 × 7) phase is grown during the oxygen adsorption only due to kinetic restrictions as already suggested by Becker *et al.*[43] As a result, the energy barrier E_{B2} to be overcome for the formation of the single layer aluminum oxide must be smaller than E_{B3}.

As shown in Fig. 8, the energy to turn the (7 × 7) metastable single layer oxide into the (√67 × √67)R12.2° bilayer oxide is even higher (E_{X2} & E_{B3}) if the process takes place by dis- and reassembling of the respective oxide phases. As a result, the (7 × 7) single layer is not converted into the (√67 × √67)R12.2° bilayer oxide during O_2 dosing. This fact ensures that the entire $Ni_3Al(111)$ surface can be covered with the (7 × 7) single layer oxide phase.

When lowering the temperature during O_2 exposure by about 20–30 K below the growth temperature of the (7 × 7) single layer aluminum oxide phase, a novel bilayer surface oxide phase is formed. This indicates that also the low temperature double layer surface oxide must be a metastable phase with a slightly lower formation energy per oxygen atom than the (7 × 7) single layer oxide phase. However, since lowering the substrate temperature leads to the formation of the novel bilayer oxide instead of the single layer oxide, an effective energy barrier E_{B1} smaller than the one to be overcome for the formation of the (7 × 7) phase has to exist. Again, once built, the bilayer oxide does not transform into the (7 × 7) single layer oxide phase during growth, because the energy required (E_{X1} & E_{B2}) exceeds E_{B1}, why the surface may be entirely covered by the low temperature bilayer oxide phase.

Note that the availability of Al atoms during surface oxide formation is transformed into a phenomenological energy barrier in the potential energy diagram of Fig. 8. For example, the formation of the single layer oxide phase within the terrace requires available Al atoms in the vicinity of the growing oxide front. If Al atoms are already exhausted from the first metal layer, diffusion from deeper layers or adatom diffusion together with a concerted place exchange is required which is mimicked as effective potential barriers in Fig. 8. As a result, the formation of the low temperature bilayer oxide phase and the single layer oxide phase results from differently balanced rate limiting processes during formation of either the growing front of the single layer oxide or the formation of a 2nd layer on top of it. The same balancing of competing growth rate events has to account for whether the (7 × 7) single layer oxide or the high temperature (√67 × √67)R12.2° double layer oxide phase is

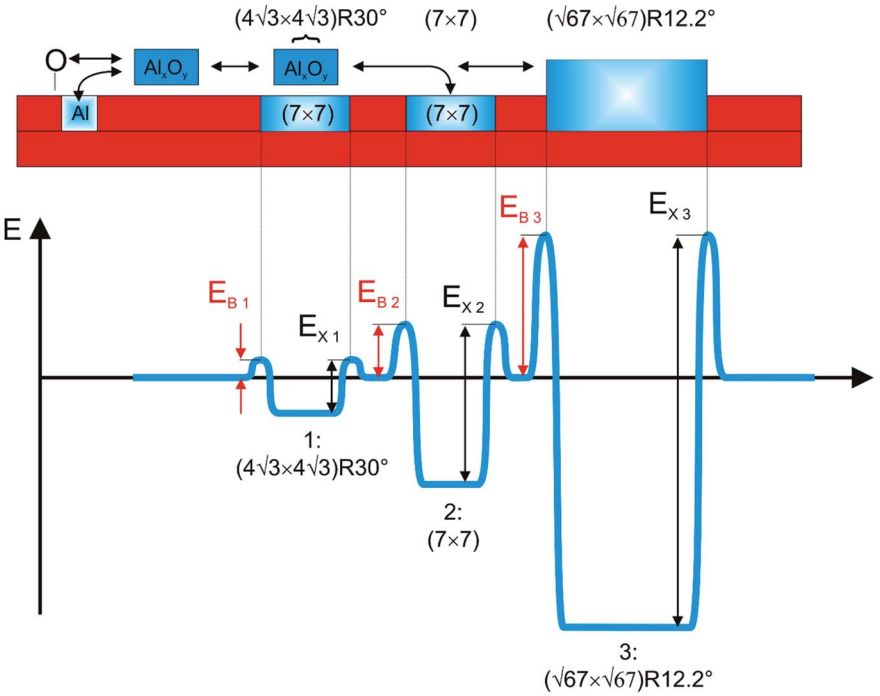

Fig. 8 Qualitative potential diagram of the formation energies per oxygen atom and the related barriers for the formation of the three different surface oxide phases: 1: $(4\sqrt{3}\times4\sqrt{3})R30^\circ$ – low temperature double layer oxide, 2: (7×7) – single layer oxide and 3: $(\sqrt{67}\times\sqrt{67})R12.2^\circ$ – high temperature double layer oxide.

formed. If the rate limiting step is the formation of a nucleus of the respective oxide phase, one expects the parallel growth of different surface oxide phases at the same time in case that nuclei already exist on the surface. This is indeed the case as can be seen in Fig. 3 confirming that already nucleated bilayer oxide islands slowly grow together with triangular patches of the (7×7) single layer oxide phase. As a result, subsequent formation of the single and the bilayer surface oxide phase can be observed only if the starting surface is extremely clean and defect free.

The growth of the different oxide phases is controlled not only by the deficiency of Al but also by the excess of metal atoms that have to be laterally displaced on the surface. The Al coverage of the (7×7) single layer oxide was shown to amount about 0.5 ML.[44] Thus, during formation of the single layer oxide 0.5 ML excess metal atoms are formed that were shown to diffuse on the terrace until they reach the ascending step edge where the single layer oxide phase is also formed. At lower temperature the time required to build the single layer phase might exceed the one of generating diffusing metal adatoms or diffusing metal–oxygen units on the surface. As a result, the concentration of such diffusing species would increase with time. If the species were trapped on top of the already built single oxide phase, naturally the 2nd layer phase will be formed due to the unbalancing of the generation and consumption rate of metal atoms on the $Ni_3Al(111)$ surface.

Note that the proposed $(4\sqrt{3}\times4\sqrt{3})R30^\circ$ unit cell of the low temperature 2nd layer oxide phase contains twice as much metal atoms as the (7×7) single layer oxide phase (*i.e.* it contains about 1 ML Al). Thus, the metal atoms are balanced when completing the 2nd layer surface oxide without having to laterally redistribute them on the terrace. The temporal trapping of excess material on the (7×7) single layer oxide islands during oxygen dosing a low temperature can be observed in Fig. 3. Here, a regular array of bright dots in registry with the moiré pattern of the (7×7) single layer oxide phase is observed in STM. The *in situ* STM experiment showed that after having dosed about 67 L oxygen most of the bright dots disappeared and the area of the 2nd layer increased more rapidly. We attribute the vanishing of the bright dot material to the fact that the formation of a second oxide layer seems to require a nucleus which is larger than the size of the resolved bright dots. Once a large enough 2nd layer nucleus exists, it soaks up the trapped material and the 2nd layer starts to grow in size. Of course, we cannot judge where the material imaged as bright dots on top of the single layer oxide originates from. One possibility is that Al atoms underneath the (7×7) single layer oxide become accessible during oxygen dosing and accumulate so that they are visible in STM. The other possibility is that they originate from alumina entities generated on the bare terrace which diffuse on the surface and get trapped on the single layer oxide patches. It is also possible that a mixture of the two processes accounts for the accumulation of second layer oxide material on the single layer oxide patches. In any case, the bright dots apparently require a pre-existing 2nd layer oxide island/nucleus in order to convert into the 2nd layer oxide.

All in all, we can summarize that the low temperature bilayer oxide with the $(4\sqrt{3}\times4\sqrt{3})R30^\circ$ oxide unit cell is formed instead of the (7×7) single layer oxide phase due to kinetic restrictions.

We should finally note that at even lower temperatures oxygen dosing also leads to second layer oxide formation as observed by *in situ* STM. Since in this case the 2nd layer oxide does not order well the LEED pattern exclusively shows the diffuse diffraction spots of the single layer oxide moiré phase. Thus, within the very narrow temperature range between 690–800 K the confusing sequence of observed diffraction patterns upon oxygen dosing follows with increasing temperature as: (7×7) moiré as disordered low temperature bilayer oxide, $(4\sqrt{3} \times 4\sqrt{3})$ R30° as ordered low temperature bilayer, again a (7×7) moiré as ordered single layer oxide and finally the $(\sqrt{67} \times \sqrt{67})$R12.2° pattern of the high temperature bilayer oxide.

Conclusions

The oxidation of the $Ni_3Al(111)$ surface was investigated within the temperature range from 690 K up to 800 K. In a combined *in situ* STM and LEED/AES study, we were able to show that with increasing oxygen dosing temperature several surface aluminum oxide structures are grown ontop of the $Ni_3Al(111)$ surface: at first a low temperature double layer oxide consisting of two A–O layers, followed by a surface oxide with only one Al–O layer and finally again a high temperature bilayer oxide. The high temperature bilayer oxide formed at 800 K is the well known $(\sqrt{67} \times \sqrt{67})$R12.2° surface oxide phase which is the thermodynamically most favorable oxide phase. The single layer surface oxide is also known in the literature as a moiré phase with a (7×7) unit cell. It is formed upon oxygen exposure at 740 K ± 10 K.

Surprisingly, at even lower growth temperature of about 720 K again a bilayer surface oxide is grown which is unknown so far. The growth of this novel low temperature bilayer oxide starts with the formation of the (7×7) single layer oxide which is subsequently covered by a second oxide layer. The surface alumina phase can be related to an α-Al_2O_3 double layer with the hexagonal oxygen lattice aligned to the substrate lattice. According to the building structure of corundum, Al honeycomb units appear in the topmost Al–O layer and lead to a diffraction pattern with a $(4\sqrt{3} \times 4\sqrt{3})$R30° unit cell when relating to the oxygen lattice of the surface oxide phase. Imaging the formation of the surface oxide by *in situ* STM shows that again kinetic restrictions relating to the availability of Al atoms account for the formation of the 2nd surface oxide layer. The low temperature 2nd layer formation takes place also at even lower temperature, but below 690 K the 2nd oxide layer is not ordered anymore. As a result, LEED only shows the (7×7) moiré pattern known from the single layer oxide. Thus, the confusing fact appears that the same LEED pattern is observed for both, a single and a double oxide layer on top of $Ni_3Al(111)$.

Conflicts of interest

There are no conflicts to declare.

Acknowledgements

The authors thank C. Becker for providing the $Ni_3Al(111)$ crystal. The work was supported through the German research foundation (DFG-INST 95/1164-1 FUGG) which is gratefully acknowledged.

References

1 A. M. Venezia and C. M. Loxton, Low pressure oxidation of Ni_3Al alloys at elevated temperatures as studied by X-ray photoelectron spectroscopy and Auger spectroscopy, *Surf. Sci.*, 1988, **194**(1), 136–148.
2 E. W. A. Young, J. C. Rivière and L. S. Welch, Investigation by X-ray photoelectron spectroscopy of the transient oxidation of NiAl, *Appl. Surf. Sci.*, 1987, **28**(1), 71–84.
3 A. Arranz and C. Palacio, Interaction of Ni/Al Interfaces with Oxygen, *Langmuir*, 2002, **18**(5), 1695–1701.
4 H. E. Evans, Cracking and spalling of protective oxide layers, *Mater. Sci. Eng., A*, 1989, **120–121**, 139–146.
5 V. Maurice, G. Despert, S. Zanna, P. Josso, M. P. Bacos and P. Marcus, The growth of protective ultra-thin alumina layers on γ-TiAl(111) intermetallic single-crystal surfaces, *Surf. Sci.*, 2005, **596**(1), 61–73.
6 R. Franchy, Growth of thin, crystalline oxide, nitride and oxynitride films on metal and metal alloy surfaces, *Surf. Sci. Rep.*, 2000, **38**(6), 195–294.
7 A. Rosenhahn, J. Schneider, C. Becker and K. Wandelt, The formation of Al_2O_3-layers on $Ni_3Al(111)$, *Appl. Surf. Sci.*, 1999, **142**(1), 169–173.
8 A. Rosenhahn, J. Schneider, C. Becker and K. Wandelt, Oxidation of $Ni_3Al(111)$ at 600, 800, and 1050 K investigated by scanning tunneling microscopy, *J. Vac. Sci. Technol., A*, 2000, **18**(4), 1923–1927.
9 T. Bertrams, A. Brodde and H. Neddermeyer, Tunneling through an epitaxial oxide film: Al_2O_3 on NiAl(110), *J. Vac. Sci. Technol., B: Microelectron. Nanometer Struct.–Process., Meas., Phenom.*, 1994, **12**(3), 2122–2124.
10 H. Isern and G. R. Castro, The initial interaction of oxygen with a NiAl(110) single crystal: A LEED and AES study, *Surf. Sci.*, 1989, **211–212**, 865–871.
11 R. M. Jaeger, H. Kuhlenbeck, H. J. Freund, M. Wuttig, W. Hoffmann, R. Franchy and H. Ibach, Formation of a well-ordered aluminium oxide overlayer by oxidation of NiAl(110), *Surf. Sci.*, 1991, **259**(3), 235–252.
12 P. Gassmann, R. Franchy and H. Ibach, Investigations on phase transitions within thin Al_2O_3 layers on NiAl(001) — HREELS on aluminum oxide films, *Surf. Sci.*, 1994, **319**(1), 95–109.
13 R. Franchy, J. Masuch and P. Gassmann, The oxidation of the NiAl(111) surface, *Appl. Surf. Sci.*, 1996, **93**(4), 317–327.
14 G. F. Cotterill, H. Niehus and D. J. O'Connor, An Stm Study of the Initial Stages of Oxidation of $Ni_3Al(110)$, *Surf. Rev. Lett.*, 1996, **03**(03), 1355–1363.
15 U. Bardi, A. Atrei and G. Rovida, Initial stages of oxidation of the Ni_3Al alloy: a study by X-ray photoelectron spectroscopy

and low energy He^+ scattering, *Surf. Sci.*, 1990, **239**(1), L511–L516.

16 W. G. Moffat, *The handbook of binary phase diagrams*, Genium Publishing Corp, New York, 1976.

17 D. R. E. Lide, *CRC Handbook of Chemistry and Physics*, CRC Press, Boca Raton, London, New York, 88th edn, 2008.

18 F. Reichel, L. P. H. Jeurgens, G. Richter and E. J. Mittemeijer, Amorphous versus crystalline state for ultrathin Al_2O_3 overgrowths on Al substrates, *J. Appl. Phys.*, 2008, **103**(9), 093515.

19 A. Beniya, N. Isomura, H. Hirata and Y. Watanabe, Lateral displacement in soft-landing process and electronic properties of size-selected Pt7 clusters on the aluminum oxide film on NiAl(110), *Chem. Phys. Lett.*, 2013, **576**, 49–54.

20 A. Beniya, N. Isomura, H. Hirata and Y. Watanabe, Morphology and chemical states of size-selected Ptn clusters on an aluminium oxide film on NiAl(110), *Phys. Chem. Chem. Phys.*, 2014, **16**(48), 26485–26492.

21 M. Baeumer and H. J. Freund, Metal deposits on well-ordered oxide films, *Prog. Surf. Sci.*, 1999, **61**, 127–198.

22 J. Libuda and H. J. Freund, Molecular beam experiments on model catalysts, *Surf. Sci. Rep.*, 2005, **57**(7), 157–298.

23 T. Worren, K. Højrup Hansen, E. Lægsgaard, F. Besenbacher and I. Stensgaard, Copper clusters on Al_2O_3/NiAl(110) studied with STM, *Surf. Sci.*, 2001, **477**(1), 8–16.

24 C.-Y. Ho, R. B. Patil, C.-C. Wang, C.-S. Chao, Y.-D. Li, H.-C. Hsu, M.-F. Luo, Y.-C. Lin, Y.-L. Lai and Y.-J. Hsu, Methanol-driven structuring of Au–Pt bimetallic nanoclusters on a thin film of Al_2O_3/NiAl(100), *Surf. Sci.*, 2012, **606**(15), 1173–1179.

25 P.-W. Hsu, Z.-H. Liao, T.-C. Hung, H. Lee, Y.-C. Wu, Y.-L. Lai, Y.-J. Hsu, Y. Lin, J.-H. Wang and M.-F. Luo, Formation and structures of Au–Rh bimetallic nanoclusters supported on a thin film of Al_2O_3/NiAl(100), *Phys. Chem. Chem. Phys.*, 2017, **19**(22), 14566–14579.

26 G.-R. Hu, C.-S. Chao, H.-W. Shiu, C.-T. Wang, W.-R. Lin, Y.-J. Hsu and M.-F. Luo, Low-temperature decomposition of methanol on Au nanoclusters supported on a thin film of Al_2O_3/NiAl(100), *Phys. Chem. Chem. Phys.*, 2011, **13**(8), 3281–3290.

27 E. Napetschnig, M. Schmid and P. Varga, Pd, Co and Co–Pd clusters on the ordered alumina film on NiAl(110): Contact angle, surface structure and composition, *Surf. Sci.*, 2007, **601**(15), 3233–3245.

28 V. Brázdová, M. V. Ganduglia-Pirovano and J. Sauer, Vanadia Aggregates on an Ultrathin Aluminum Oxide Film on NiAl(110), *J. Phys. Chem. C*, 2010, **114**(11), 4983–4994.

29 A. Desikusumastuti, Z. Qin, T. Staudt, M. Happel, Y. Lykhach, M. Laurin, S. Shaikhutdinov and J. Libuda, Controlling metal/oxide interactions in bifunctional nanostructured model catalysts: Pd and BaO on Al_2O_3/NiAl(110), *Surf. Sci.*, 2009, **603**(1), L9–L13.

30 R. V. Mom, M. J. Rost, J. W. M. Frenken and I. M. N. Groot, Tuning the Properties of Molybdenum Oxide on Al_2O_3/NiAl(110): Metal versus Oxide Deposition, *J. Phys. Chem. C*, 2016, **120**(35), 19737–19743.

31 S. Addepalli, N. P. Magtoto and J. A. Kelber, Interactions at the $Ni_3Al(111)$–S–Al_2O_3 Interface at Elevated Temperatures: Ordering of Al_2O_3 on an S-Modified Substrate, *Langmuir*, 2000, **16**(22), 8352–8359.

32 N. P. Magtoto, C. Niu, M. Anzaldua, J. A. Kelber and D. R. Jennison, STM-induced void formation at the Al_2O_3/$Ni_3Al(111)$ interface, *Surf. Sci.*, 2001, **472**(3), L157–L163.

33 S. Degen, A. Krupski, M. Kralj, A. Langner, C. Becker, M. Sokolowski and K. Wandelt, Determination of the coincidence lattice of an ultra thin Al_2O_3 film on $Ni_3Al(111)$, *Surf. Sci.*, 2005, **576**(1), L57–L64.

34 M. Schmid, G. Kresse, A. Buchsbaum, E. Napetschnig, S. Gritschneder, M. Reichling and P. Varga, Nanotemplate with Holes: Ultrathin Alumina on $Ni_3Al(111)$, *Phys. Rev. Lett.*, 2007, **99**(19), 196104.

35 T. Maroutian, S. Degen, C. Becker, K. Wandelt and R. Berndt, Superstructures and coincidences of a thin oxide film on a metallic substrate: a STM study, *Phys. Rev. B: Condens. Matter Mater. Phys.*, 2003, **68**(15), 155414.

36 S. Gritschneder, C. Becker, K. Wandelt and M. Reichling, Disorder or Complexity? Understanding a Nanoscale Template Structure on Alumina, *J. Am. Chem. Soc.*, 2007, **129**(16), 4925–4928.

37 A. Wiltner, A. Rosenhahn, J. Schneider, C. Becker, P. Pervan, M. Milun, M. Kralj and K. Wandelt, Growth of copper and vanadium on a thin Al_2O_3-film on $Ni_3Al(111)$, *Thin Solid Films*, 2001, **400**(1), 71–75.

38 A. Bailly, G. Sitja, M.-C. Saint-Lager, S. Le Moal, F. Leroy, M. De Santis, C. R. Henry and O. Robach, Influence of Palladium on the Ordering, Final Size, and Composition of Pd–Au Nanoparticle Arrays, *J. Phys. Chem. C*, 2017, **121**(46), 25864–25874.

39 J. A. Olmos-Asar, E. Vesselli, A. Baldereschi and M. Peressi, Self-seeded nucleation of Cu nanoclusters on Al_2O_3/$Ni_3Al(111)$: an ab initio investigation, *Phys. Chem. Chem. Phys.*, 2014, **16**(42), 23134–23142.

40 J. A. Olmos-Asar, E. Vesselli, A. Baldereschi and M. Peressi, Towards optimal seeding for the synthesis of ordered nanoparticle arrays on alumina/$Ni_3Al(111)$, *Phys. Chem. Chem. Phys.*, 2015, **17**(42), 28154–28161.

41 E. Vesselli and M. Peressi, Chapter 8 – Nanoscale Control of Metal Clusters on Templating Supports, in *Studies in Surface Science and Catalysis*, ed. P. Fornasiero and M. Cargnello, Elsevier, 2017. pp. 285–315.

42 E. Vesselli, A. Baraldi, S. Lizzit and G. Comelli, Large Interlayer Relaxation at a Metal-Oxide Interface: The Case of a Supported Ultrathin Alumina Film, *Phys. Rev. Lett.*, 2010, **105**(4), 046102.

43 C. Becker, J. Kandler, H. Raaf, R. Linke, T. Pelster, M. Dräger, M. Tanemura and K. Wandelt, Oxygen adsorption and oxide formation on Ni_3Al (111), *J. Vac. Sci. Technol., A*, 1998, **16**(3), 1000–1005.

44 X. Ma and S. Günther, Imaging the confined surface oxidation of $Ni_3Al(111)$ by in situ high temperature scanning tunneling microscopy, *Phys. Chem. Chem. Phys.*, 2018, **20**(34), 21844–21855.

45 J. A. Kelber, Alumina surfaces and interfaces under non-ultrahigh vacuum conditions, *Surf. Sci. Rep.*, 2007, **62**(7), 271–303.

46 F. Qin, N. P. Magtoto and J. A. Kelber, H_2O-induced instability of $Al_2O_3/Ni_3Al(110)$ and $Al_2O_3/Ni_3Al(111)$ thin films under non-UHV conditions, *Surf. Sci.*, 2004, **565**(2), L277–L282.

47 J. Stöhr, L. I. Johansson, S. Brennan, M. Hecht and J. N. Miller, Surface extended-x-ray-absorption-fine-structure study of oxygen interaction with Al(111) surfaces, *Phys. Rev. B: Condens. Matter Mater. Phys.*, 1980, **22**(8), 4052–4065.

48 J. Toofan and P. R. Watson, The termination of the α-Al_2O_3 (0001) surface: a LEED crystallography determination, *Surf. Sci.*, 1998, **401**(2), 162–172.

49 M. C. Biesinger, L. W. M. Lau, A. R. Gerson and R. S. C. Smart, The role of the Auger parameter in XPS studies of nickel metal, halides and oxides, *Phys. Chem. Chem. Phys.*, 2012, **14**(7), 2434–2442.